

Behavior of Texture Formation during Uniaxial Compression of AA5052 and AA5182 Alloys at High Temperatures

Hyeon-Mook Jeong, Kazuto Okayasu and Hiroshi Fukutomi

Yokohama National University, 79-5, Tokiwadai, Hodogaya-ku, Yokohama 240-8501, Japan

In order to understand the mechanism of texture formation in commercial aluminum alloys during high temperature deformation, uniaxial compressive deformation is conducted at various temperatures under various strain rates up to a strain of -1.0 in AA5052 and AA5182 alloys. Fiber textures are formed in all the deformation conditions. It is found that the main component of the fiber texture is $\{001\}$, $\{011\}$, or $\{001\}+\{011\}$ which varies depending on the deformation conditions. The main component of the fiber texture and its intensity are compared with those for the binary Al-Mg alloys. On the basis of the relationship between texture and deformation condition, $\{001\}$ texture map is constructed for AA5052 aluminum alloy.

Keywords: *Texture, EBSD, High temperature compressive deformation, Grain boundary migration, AA5052, AA5182*

1. Introduction

In recent years, texture of aluminum alloys has been investigated for the improvement of their workability. It is known that texture has effects on plastic workability such as deep drawing and bending [1, 2]. In the previous papers, two of the authors and other researchers reported that texture formation depended strongly on the deformation condition which could be related with the deformation mechanisms at high temperatures in binary Al-Mg alloys [3-5]. There are, however, few reports on texture formation at high temperature deformation on the commercial aluminum alloys which is important for the practical application of the findings on Al-Mg binary alloys. In this study, the texture formation of commercial Al-Mg alloys, AA5052 and AA5182 are experimentally investigated by uniaxial compression deformation at high temperatures.

2. Experimental Procedures

AA5052 and AA5182 alloys were provided by Nippon Light Metal Co., Ltd. and Furukawa-Sky Aluminum Corp. in the form of hot rolled plate with 20mm in thickness. Cylindrical specimens with various sizes were prepared by spark erosion machining for compression tests. Aspect ratio of specimens was kept at 1.5 for all sizes of specimens. The specimens of AA5052 alloy were annealed at 853K for 100min in air. The specimens of AA5182 alloy were annealed at 843K for 1000min, followed by the further annealing at 773K for 50min in air. Both specimens were quenched into water after the annealing. The chemical compositions of the specimens are given in Table 1. Electron back-scattered diffraction (EBSD) observation clarified that the grains were equiaxed and the random textures were formed before deformation in both specimens.

Uniaxial compression tests were conducted under constant crosshead speed conditions in air. The ranges of temperature and strain rate were from 673K to 823K and from 5.0×10^{-4} to $5.0 \times 10^{-2} \text{s}^{-1}$, respectively. Final strain rate was evaluated on the basis of crosshead speed and the height of specimens. The infrared ray furnace was used for heating. Specimens were kept for 1h at the test temperatures before deformation to decrease the influence of thermal expansion during deformation. After the deformation, the furnace was immediately opened and the power supply was switched off simultaneously, and then specimens were quenched into water, in order to prevent the change in microstructure after high temperature compression test.

After the compression tests, the mid-plane sections of the specimens were prepared by mechanical and electrolytic polishing for texture and EBSD measurements. Texture measurements were conducted by the Schulz reflection method using nickel filtered copper K_{α} radiation. $\{001\}$, $\{011\}$, and $\{111\}$ pole figures were constructed, using diffracted X-ray intensities measured on 111, 200, and 220 reflections. Based on these pole figures, orientation distribution function (ODF) was calculated by the Dahms-Bunge method [6]. Textures were examined on the basis of pole figures and inverse pole figures derived from ODF. Local crystal orientations were measured by the EBSD system equipped on JEOL JSM-5600 scanning electron microscope. The measurements were performed every $4\mu\text{m}$.

Table 1 Chemical composition of AA5052 and AA5182 alloys in the present study (mass%)

	Mg	Fe	Cr	Mn	Si	Cu	Zn	Ti	Al
AA5052	2.58	0.28	0.18	0.01	0.08	0.01	0.01	0.02	bal.
AA5182	4.54	0.30	0.04	0.45	0.12	0.09	—	0.04	bal.

3. Results

3.1 Stress – strain curves

Figure 1 shows the true stress – true strain curves for the deformation of AA5052 and AA5182 alloys up to a true strain of -1.0 at temperatures and strain rates of (a) 723K, $5.0 \times 10^{-2} \text{s}^{-1}$, (b) 723K, $5.0 \times 10^{-3} \text{s}^{-1}$ and (c) 823K, $5.0 \times 10^{-3} \text{s}^{-1}$, respectively. The high temperature yielding phenomena are observed in all the cases. Flow stresses of both alloys increase with decreasing temperature and increasing strain rate.

3.2 Texture formation

Figures 2 (a) and (b) show $\{111\}$ pole figures of AA5052 alloy after the deformation at (a) 823K and (b) 723K with a strain rate of $5.0 \times 10^{-2} \text{s}^{-1}$ up to a strain of -1.0 , respectively. Pole densities are projected onto the compression plane. The average pole density is used as a unit. The pole density is distributed in a concentric circular manner in both figures. This means the formation of fiber textures. In the present study, formation of fiber texture was confirmed for all deformation conditions. In Fig. 2 (a), the area of high pole density appears between 35 and 55 degrees away from the center. In Fig. 2 (b), the area of high pole density appears about 35 degrees away from the center. This means that the main components of textures are different in these two specimens. These characteristics are also observed in AA5182 alloy. The main component of fiber texture was examined based on the basis of ODF. Figure 3 shows the inverse pole figures showing the spatial distribution of poles for compression planes on the specimens deformed at 823K((a) and (c)) and 723K((b) and (d)) under a final strain rate of $5.0 \times 10^{-2} \text{s}^{-1}$ up to a strain of -1.0 . (a), (b) and (c), (d) show the results of AA5052 and AA5182 alloys, respectively. Again, the average pole density is used as a

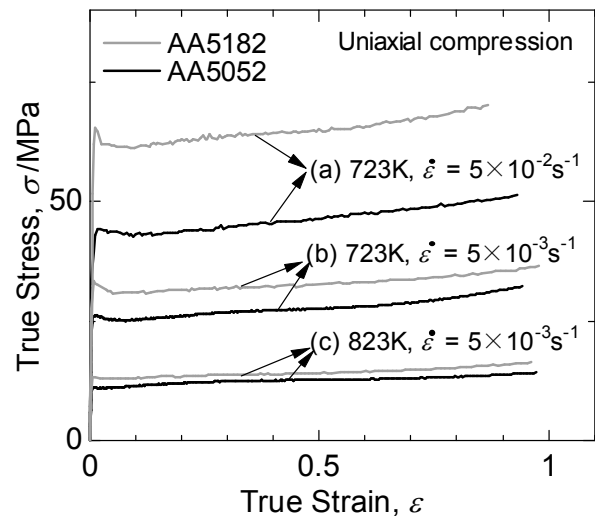


Fig. 1 True stress-true strain curves of AA5052(black lines) and AA5182(gray lines) alloys obtained by compression test up to a strain of -1.0 . The deformation is conducted under (a) 723K with a strain rate of $5.0 \times 10^{-2} \text{s}^{-1}$, (b) 723K with a strain rate of $5.0 \times 10^{-3} \text{s}^{-1}$ and (c) 823K with a strain rate of $5.0 \times 10^{-3} \text{s}^{-1}$, respectively.

unit for drawing the contour lines. The main component of texture in both alloys changes from $\{011\}$ to $\{001\}$ with increasing temperature. The pole densities at (001) and (011) are given below the inverse pole figure as $P(001)$ and $P(011)$, respectively. The pole density at (001) increases from 2.7 to 7.7 times of the random level with increasing temperature in AA5052 alloy. In the same deformation condition, the pole density at (001) for AA5182 alloy also increases from 1.6 to 10. This means that the main component of texture and the sharpness of $\{001\}$ texture vary depending on temperature and composition.

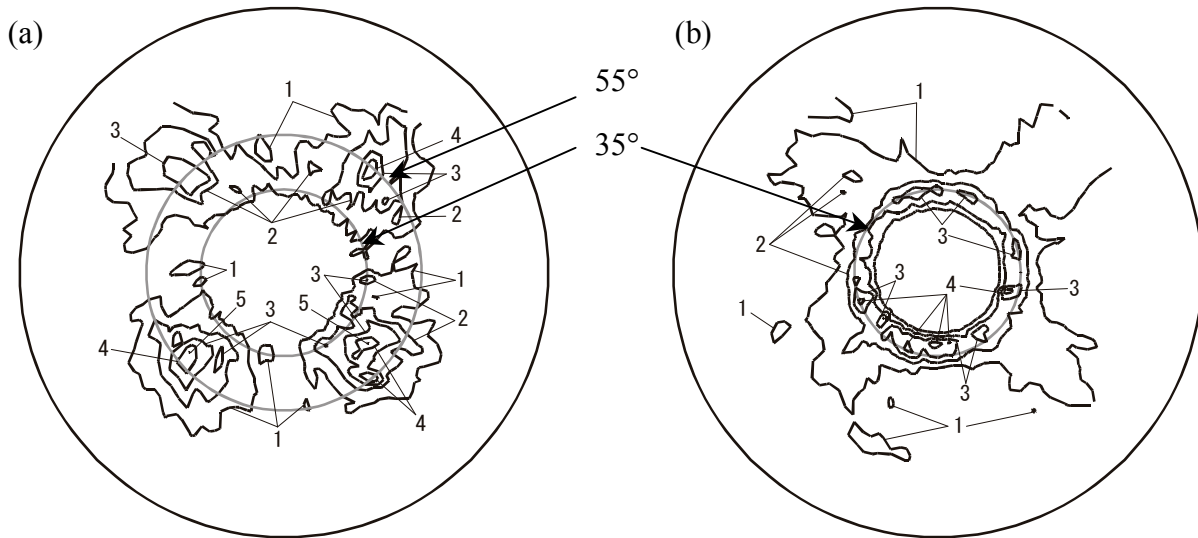


Fig. 2 $\{111\}$ pole figures for AA5052 alloy compressed at (a) 823K and (b) 723K under a final strain rate of $5.0 \times 10^{-2} \text{ s}^{-1}$ up to a strain of -1.0 . The pole density is projected onto the compression plane. The average pole density is used as a unit.

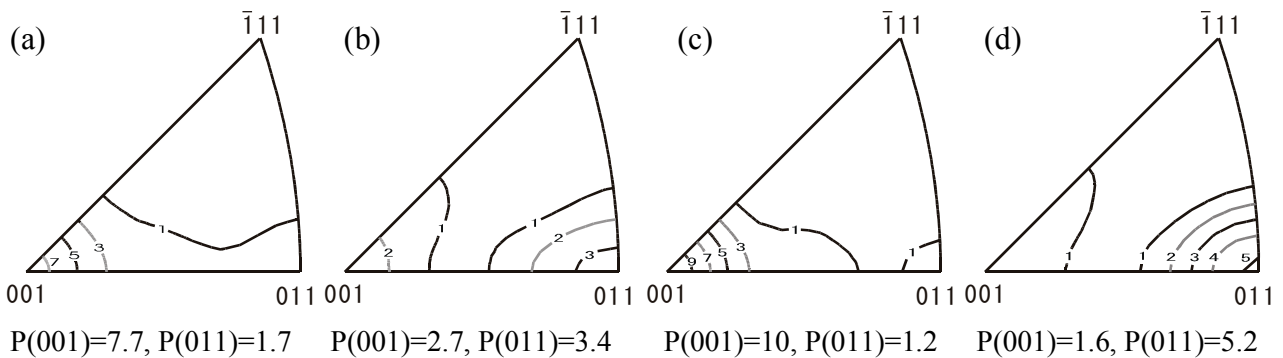


Fig. 3 Inverse pole figures for the specimens compressed at 823K((a), (c)) and 723K((b), (d)) under a final strain rate of $5.0 \times 10^{-2} \text{ s}^{-1}$ up to a strain of -1.0 . (a)~(b) and (c)~(d) show the results of AA5052 and AA5182 alloys, respectively. The distributions of pole densities of the compression plane are given. The average pole density is used as a unit. The pole densities at (001) and (011) are given below the figures.

3.3 Grain structures

Figure 4 shows the grain structure maps of AA5052 alloy after the deformation at (a) 823K and (b) 723K under a final strain rate of $5.0 \times 10^{-2} \text{ s}^{-1}$ up to a strain of -1.0 . The map is constructed on the mid-plane section by EBSD measurement. When the minimum rotation angle between the neighboring points of measurements is larger than 15 degrees, grain boundaries are drawn by black

lines. The grains are marked with dark and light gray colors when the orientations of compression planes are within 15 degrees from $\{001\}$ and $\{011\}$, respectively. In Fig 4(a), it was found that the grains with $\{001\}$ orientation were 55% of the area, whereas area fraction of $\{011\}$ was 14%. In this case, it is seen that the size of $\{001\}$ grains is larger than that of the other orientations. Different from Fig. 4(a), the area fractions of $\{001\}$ and $\{011\}$ in Fig. 4(b) are 22% and 46%, respectively. In this case, the grains with $\{011\}$ orientation are much larger than those of the other orientations.

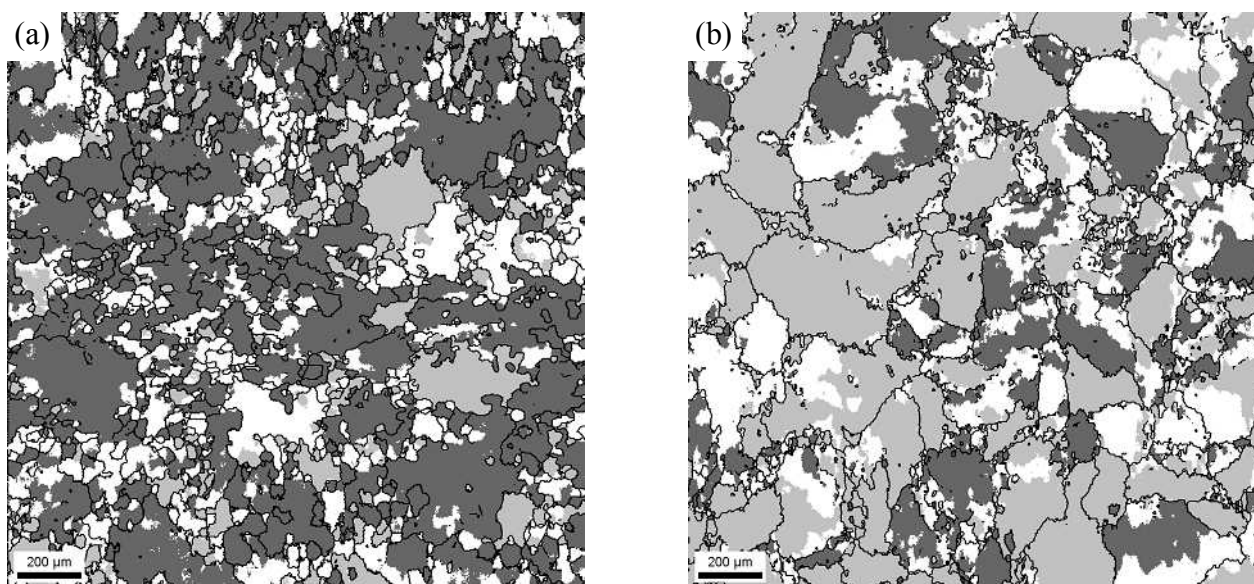


Fig. 4 Grain structure maps for the compression plane of AA5052 alloy derived from EBSD measurement. The deformations are conducted with a strain rate of $5.0 \times 10^{-2} \text{ s}^{-1}$ at (a) 823K and (b) 723K, respectively. The dark gray grains are within 15 degrees from $\{001\}$ (compression plane) orientation and light gray grains are within 15 degrees from $\{011\}$ orientation. Black lines are high angle grain boundaries with a misorientation angle greater than 15 degrees.

4. Discussion

4.1 Texture formation in commercial alloys

Okayasu *et al.* investigated the texture formation during the high temperature deformation of Al-3Mg and Al-3Mg-0.2Sc alloys [7]. It was found that the formation of $\{001\}$ texture in Al-3Mg-0.2Sc alloy was remarkably retarded by Al_3Sc precipitates. This suggests that the grain boundary migration contributes to the development of $\{001\}$ texture. As shown in Fig. 3, when the temperature increases from 723K to 823K, the sharpness of $\{001\}$ component increases irrespective of the kind of alloys. This can be understood by the consideration that the preferential growth of $\{001\}$ grains by grain boundary migration drives the development of $\{001\}$ texture in both alloys. The microstructure given in Fig. 4(a) coincides with this consideration: $\{001\}$ grains grow by consuming $\{011\}$ grains.

As shown in Table 1, AA5052 and AA5182 alloys are the commercial alloys containing about 2.5 and 4.5 mass% Mg, respectively. Figures 5(a) to (d) are the inverse pole figures examined after deformation of (a) Al-3Mg, (b) AA5052, (c) Al-5Mg and (d) AA5182 alloys, respectively. Deformation is conducted at 723K under a strain rate of $5.0 \times 10^{-4} \text{ s}^{-1}$ up to a strain of -1.0 . In Figs. 5(a) and (c), it is seen that the sharpness of $\{001\}$ texture is enhanced by an increase in magnesium concentration at the same deformation condition. It is also found that the pole density at $\{001\}$ of AA5182 alloy is higher than that of AA5052 alloy. Nakashima *et al.* investigated the mobility of edge

dislocation in Al-Mg solution alloys at high temperatures [8]. They reported that the mobility of edge dislocation decreases in an exponential manner in aluminum alloys containing higher solute concentration. Thus, it is considered that the solute atoms retard the formation of subgrain in the crystal grains, resulting in the enhancement of the orientation dependence of stored energy, which accelerates the growth of grains with $\{001\}$ orientations.

Comparison of Figs. 5(a) with (b) shows that the pole density at (001) for the commercial AA5052 alloy is lower than that of binary Al-3Mg alloy. Figures 5(c) and (d) also show the same tendency. This suggests that alloy elements other than aluminum and magnesium in the commercial aluminum alloys may suppress the grain boundary migration.

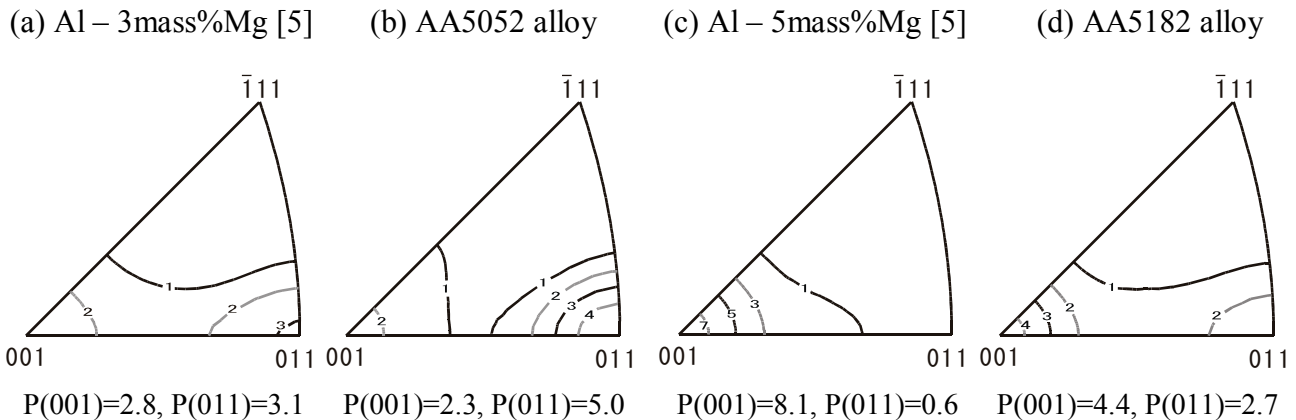


Fig. 5 Inverse pole figures for compression planes of (a) Al-3Mg [5], (b) AA5052, (c) Al-5Mg [5] and (d) AA5182 alloys compressed at 723K under a final strain rate of $5.0 \times 10^{-4} \text{ s}^{-1}$ up to a strain of -1.0 . The average density is used as a unit. The pole densities at (001) and (011) are given below the figures.

4.2 $\{001\}$ texture map in AA5052 alloy

As previously described, the main component of textures and grain structure vary depending on deformation conditions. The $\{001\}$ grains with an indented shape occupy 55% of the area in Fig. 4(a). This suggests that grain boundary migration enhances the development of $\{001\}$ texture. In contrast, $\{011\}$ grains occupy 46% of the whole area in Fig. 4(b). It is considered that the large grains with $\{011\}$ orientations are formed by the compression deformation with crystal rotation due to $\{111\} \langle 110 \rangle$ slip. In order to elucidate the change of the pole density in relating to the deformation conditions, the pole densities at (001) of AA5052 alloy are plotted as a function of strain rates and temperatures in Fig. 6. Vertical and horizontal axes are strain rate and reciprocal absolute temperature, respectively. The solid circles are the deformation conditions. The numerical value under the solid circles expresses the pole density at (001) in the inverse pole figures. From these pole densities, contour lines for pole densities at (001) are drawn by gray solid lines for the levels of 1, 3, 5 and 7. The area of level 7 appears at 823K with higher strain rates. This tendency was also seen in AA5182 alloy; the maximum pole density was higher than AA5052 alloy as 12 times of random level, which appeared at 823K under final strain rate of $5.0 \times 10^{-3} \text{ s}^{-1}$ [9].

5. Conclusions

In order to elucidate the behavior of texture formation during high temperature deformation of AA5052 and AA5182 alloys, uniaxial compression deformation is conducted under various temperatures and strain rates. The major results are summarized as follows.

- (1) The main component of fiber texture depends on the deformation conditions in these commercial alloys.
- (2) The pole densities at (001) in the present alloys are much weaker than those of the binary alloys with similar solute concentration at the same deformation conditions. This might be attributed to the suppression of grain boundary migration.
- (3) For understanding the behavior of texture formation, {001} texture map is constructed as a function of deformation temperatures and strain rates in AA5052 alloy.

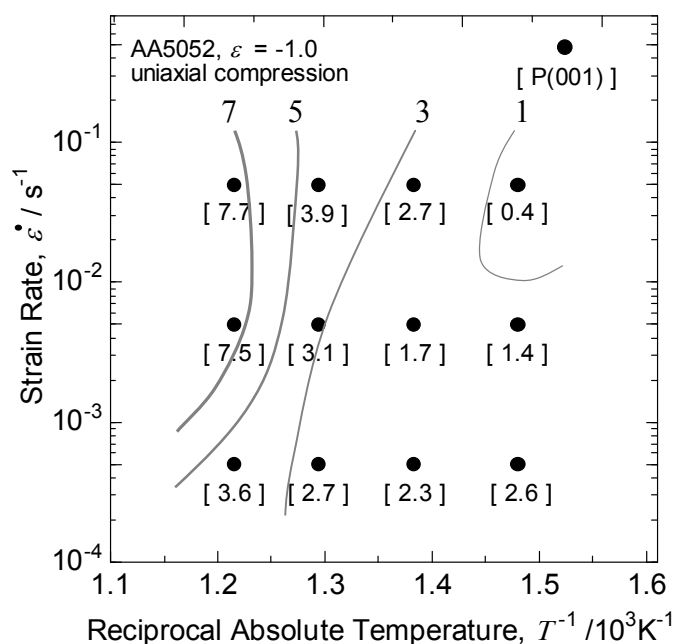


Fig. 6 Effects of deformation temperature and strain rates on the development of {001} components of the texture for AA5052 alloy. The gray lines show the contour for the pole density of (001) ({001} texture map).

Acknowledgements

The authors appreciate to The Japan Light Metal Educational Foundation, Inc. for the financial support.

References

- [1] H. Inoue and T. Takasugi: *Mater. Trans.* 48 (2007) 2014–2022.
- [2] S. Ikawa, M. Asano and S. Hirano: *Abstracts of the 116th Annual Meeting of the Japan Institute of Light Metals* (2009) 301-302. (in Japanese).
- [3] K. Okayasu, H. Takekoshi and H. Fukutomi: *Mater. Trans.* 48 (2007) 2002-2007.
- [4] S. R. Chen and U. F. Kocks: *Hot Deformation of Aluminum Alloys*, ed. by T. G. Langdon, H. D. Merchant, J. G. Morris and M. A. Zaidi, (The Minerals, Metals and Materials Society, 1991) pp. 89–104.
- [5] K. Okayasu and H. Fukutomi: *J. Japan Inst. Metals* 73 (2009) 58–63. (in Japanese)
- [6] M. Dahms and H. J. Bunge: *J. Appl. Crystallogr.* 22 (1989) 439-447.
- [7] K. Okayasu and H. Fukutomi: *J. Japan Inst. Metals* 70 (2006) 562–567. (in Japanese)
- [8] H. Nakashima and H. Yoshinaga: *J. Japan Inst. Metals* 56 (1992) 254-261. (in Japanese)
- [9] H. M. Jeong, K. Okayasu and H. Fukutomi: submitted to *Mater. Trans.* (2010).